Available online at www.sciencedirect.com
ScienceDirect
Journal of Computational Physics 222 (2007) 809–831
JOURNAL OF COMPUTATIONAL PHYSICS
www.elsevier.com/locate/jcp

Performance analysis and optimization of finite-difference schemes for wave propagation problems

Sergio Pirozzoli *

Università degli Studi di Roma "La Sapienza", Dipartimento di Meccanica e Aeronautica, Via Eudossiana 18, 00184 Roma, Italy

Received 22 December 2005; received in revised form 14 August 2006; accepted 21 August 2006
Available online 2 October 2006

Abstract

In the present paper, we gauge the performance of finite-difference schemes with Runge–Kutta time integration for wave propagation problems by rigorously defining appropriate cost and error metrics in a simple setting represented by the linear advection equation. Optimal values of the grid spacing and of the time step are obtained as a result of a cost minimization (for given error level) procedure. The theory suggests superior performance of high-order schemes when highly accurate solutions are sought for, and in several space dimensions even more. The analysis of the global discretization error shows the occurrence of two (approximately independent) sources of error, associated with the space and time discretizations. The improvement of the performance of finite-difference schemes can then be achieved by trying to separately minimize the two contributions. General guidelines for the design of problem-tailored, optimized schemes are provided, suggesting that significant reductions of the computational cost are in principle possible. The application of the analysis to wave propagation problems in a two-dimensional environment demonstrates that the analysis carried out for the scalar case directly applies to the propagation of monochromatic sound waves. For problems of sound propagation involving disparate length-scales the analysis still provides useful insight for the optimal exploitation of computational resources; however, the actual advantage provided by optimized schemes is not as evident as in the single-scale, scalar case.

Keywords: Computational aeroacoustics; Compact schemes; Optimized schemes

1. Introduction

Computational aeroacoustics and direct numerical simulation of compressible turbulence require the use of high-fidelity numerical schemes, which must be capable to resolve a broad range of length scales, often orders of magnitude apart. For this purpose compact schemes have been developed, [8] which guarantee spectral-like resolution properties, are cheaper to use than spectral and pseudo-spectral schemes and are easier to handle, especially when non-trivial geometries are involved. It is well known [12] that the order of the truncation error of a numerical scheme only provides informations on the asymptotic convergence rate to the exact solution,

* Tel.: +39 06 44585202; fax: +39 06 4881759.
E-mail address: sergio.pirozzoli@uniroma1.it.

0021-9991/$ - see front matter
doi:10.1016/j.jcp.2006.08.006

but it does not convey any information on the actual error on a finite computational grid; rather, wave-propagation characteristics of a difference scheme provide informations on all the Fourier components supported on the grid. As a result of Fourier analysis, optimized (or dispersion–relation–preserving, DRP) finite-difference schemes have been developed [11,9], which are capable to accurately resolve harmonic components with few points-per-wavelength.

The issue of the computational efficiency of finite-difference schemes has been investigated in detail by Colonius and Lele [2]; those authors considered the behavior of several types of spatial discretizations, implicitly assuming exact time integration, and concluded that for normalized errors (defined as the relative error between the exact and modified wavenumber) less than about 1% optimized schemes, and in particular the sixth-order pentadiagonal optimized scheme of Lui and Lele [9], are most efficient despite a higher operation count compared to non-optimized ones. The error associated with approximate time integration (generally performed by means of Runge–Kutta or Linear Multi-step time marching methods) is usually considered separately from the spatial error [2]. Hu et al. [7] have developed optimized Runge–Kutta schemes, which attempt to minimize the integrated dispersion and dissipation errors associated with time integration over a certain range of Courant numbers.

In the present paper, we attempt to develop a general strategy for the analysis of the efficiency of finite-difference schemes for wave propagation problems, trying to involve time integration in the analysis in a natural way. For this purpose we proceed by rigorously defining error and cost metrics for the one-dimensional linear advection equation, and show that appropriate choices for the grid spacing and the time step naturally stem from a cost minimization procedure for a given error level; such optimal choice depends upon both the physical parameters of the problem and on the accuracy requirements. The analysis also leads to rational and simple criteria for deriving optimized space- and time-discretization schemes, based on concepts similar to that of 'resolving efficiency' introduced by Lele. A careful design of the space- and time-discretization schemes, as well as an appropriate choice of the grid spacing and of the time step can yield substantial computer time savings, which could help CFD and CAA practitioners. The main focus of the present paper is on assessing the wave propagation features of finite-difference schemes; accordingly, the effects of nonlinearities and of boundary conditions, which are extremely important for the accuracy and stability of numerical algorithms for practical calculations (see, e.g. Ref. [1] for a comprehensive review), are not addressed, and left for future work. Weak nonlinearities can in principle be accounted for, as shown in Section 2.4, even though quantitative assessment of the theory in that case is made difficult by the lack of exact solutions.

The paper is organized as follows: in Section 2 we rigorously define cost and error metrics for wave propagation problems using the linear advection equation as a model, and search for optimal performance of finite-difference schemes; in Section 3 we compare the performance of various explicit and compact schemes, and address the effect of the problem dimensionality; in Section 4 we analyze the contribution of space and time discretization to the global error; in Section 5 we present general guidelines for the optimization of space and time-discretization schemes; finally, in Section 6 we present results of numerical simulations of the two-dimensional acoustics equations, and show comparison with theoretical predictions.

2. Performance analysis of finite-difference schemes

In order to arrive at simple predictive formulas we consider (as customary in the literature) as a model problem the linear advection equation in an unbounded (one-dimensional) domain

$$u_t + au_x = 0, \quad -\infty < x < +\infty, \quad u(x,0) = u_0(x), \tag{1}$$

and assume $a > 0$. We additionally assume sinusoidal monochromatic initial conditions with wavelength λ (and wavenumber $w = 2\pi/\lambda$),

$$u_0(x) = \hat{u}_0 \mathrm{e}^{\mathrm{i}wx}. \tag{2}$$

Let us consider the discretization of Eq. (1) on a uniform grid with spatial spacing h and time step k; the exact solution of Eq. (1) at time $T = nk$ is

$$u(x,T) = \hat{u}_n \mathrm{e}^{\mathrm{i}wx}, \tag{3}$$

with

$$\hat{u}_n = \mathrm{e}^{-\mathrm{i}n\sigma\varphi}\hat{u}_0, \tag{4}$$

where $\varphi = wh$ ($-\pi \leqslant \varphi \leqslant \pi$) is the reduced wavenumber, and $\sigma = ak/h$ is the Courant number. A linear finite difference approximation of Eq. (1) yields instead an approximate solution [12,8,2]

$$v(x,T) = \hat{v}_n \mathrm{e}^{\mathrm{i}wx}, \tag{5}$$

with

$$\hat{v}_n = g^n \hat{u}_0, \tag{6}$$

where $g = g(\varphi,\sigma)$ is the amplification factor of the difference scheme [6], which depends both upon the space and time discretizations. Considering approximations of the spatial derivative of v ($v' \approx \partial v/\partial x$) of the type

$$\sum_{L=-Q}^{R} \alpha_L v'_{j+L} = \frac{1}{h}\sum_{l=-q}^{r} a_l v_{j+l}, \tag{7}$$

and an s-stage Runge–Kutta scheme for time integration, one has [7]

$$g(\varphi,\sigma) = \sum_{m=0}^{s} \gamma_m (-\mathrm{i}\sigma\Phi(\varphi))^m, \tag{8}$$

where the coefficients γ_m are related to the coefficients of the Runge–Kutta scheme, and where

$$\Phi(\varphi) = \frac{1}{i}\frac{\sum_{l=-q}^{r} a_l \mathrm{e}^{\mathrm{i}l\varphi}}{\sum_{L=-Q}^{R} \alpha_L \mathrm{e}^{\mathrm{i}L\varphi}}, \tag{9}$$

is the modified wavenumber [8] associated with the spatial discretization. The coefficients α_L, a_l that appear in Eq. (7) may be chosen either to minimize the truncation error, thus yielding $v'_j = \partial v/\partial x(x_j) + \mathrm{O}(h^{Q+R+q+r})$, or else to optimize the behavior in wavenumber space so as to have $\Phi \approx \varphi$ [11,9], at the expense of the formal order of accuracy. In the following we will denote non-optimized spatial discretizations with the symbol CQRqr (for example, C0011 corresponds to the second-order explicit central scheme), and consider the Lui and Lele scheme [9] as representative of optimized schemes. With regard to time integration, the coefficients γ_m in Eq. (8) may be either chosen to minimize the truncation error, thus having $\gamma_m = 1/m!$, or to minimize the dissipation and dispersion error, as done by Hu et al. [7]. Non-optimized, sth order Runge–Kutta schemes will be labeled in the following as RKs.

2.1. Definition of an error metric

We define the solution error as the distance in L_2 norm of the approximate solution from the exact solution at time T

$$\begin{aligned} |v(\cdot,T) - u(\cdot,T)|_2 &= \left(\frac{1}{\lambda}\int_{x_0}^{x_0+\lambda} |v(x,T) - u(x,T)|^2 \,\mathrm{d}x\right)^{1/2} = |\hat{v}_n - \hat{u}_n| = |g^n - \mathrm{e}^{-\mathrm{i}n\sigma\varphi}||\hat{u}_0| \\ &= |g^n - \mathrm{e}^{-\mathrm{i}n\sigma\varphi}||u_0(\cdot)|_2. \end{aligned} \tag{10}$$

Let $\delta g \equiv g - \mathrm{e}^{-\mathrm{i}\sigma\varphi}$ be the difference between the approximate and the exact amplification factor, one has

$$g^n = (\mathrm{e}^{-\mathrm{i}\sigma\varphi} + \delta g)^n = \mathrm{e}^{-\mathrm{i}n\sigma\varphi}(1 + \delta g \mathrm{e}^{\mathrm{i}\sigma\varphi})^n \approx \mathrm{e}^{-\mathrm{i}n\sigma\varphi}(1 + n\delta g \mathrm{e}^{\mathrm{i}\sigma\varphi}), \tag{11}$$

having assumed $|\delta g| \ll 1$; such assumption is satisfied by any reasonably accurate scheme, and can be checked a posteriori. We then obtain

$$g^n - \mathrm{e}^{-\mathrm{i}n\sigma\varphi} \approx n\delta g \mathrm{e}^{-\mathrm{i}(n-1)\sigma\varphi}, \tag{12}$$

and finally

$$|g^n - e^{-in\sigma\varphi}| \approx n \cdot |g(\varphi,\sigma) - e^{-i\sigma\varphi}|. \tag{13}$$

We define the relative error at time T as

$$E = \frac{|v(\cdot,T) - u(\cdot,T)|_2}{|u_0(\cdot)|_2} \approx (awT) \cdot \frac{|g(\varphi,\sigma) - e^{-i\sigma\varphi}|}{\sigma\varphi}, \tag{14}$$

having noticed that $n = (awT)/(\sigma\varphi)$.

2.2. Definition of a cost metric

For the purpose of consistently defining a cost metric, we assume [2] that the computational cost is

(1) proportional to the total number of points, i.e. L/h, where L is the size of the computational domain;
(2) proportional to the number of operations/node required by the spatial discretization scheme, say N_{op};
(3) proportional to the number of Runge–Kutta stages, s;
(4) proportional to the number of time steps, $n = T/k$,

thus yielding

$$C \sim sN_{op}TL\frac{1}{kh} = sN_{op} \cdot (awT) \cdot (wL) \cdot \frac{1}{\sigma\varphi^2}. \tag{15}$$

In the present work we have borrowed the estimates of the operation count (in terms of floating point operations/node) reported by Colonius and Lele (see Table 2 of Ref. [2]).

2.3. Optimal performance for single-scale problems

We point out that in Eqs. (14) and (15) the non-dimensional groups awT (which is a measure of the number of wavelengths traveled by the wave in a time interval T) and wL (which is a measure of the number of wavelengths contained in the computational domain) are dictated only by the problem under consideration, while the space and time discretization enter through s, N_{op} and $g(\varphi,\sigma)$. The analysis of the performance of finite-difference schemes for a given physical problem (i.e. for given values of awT, wL) can then be carried out in terms of normalized error and cost functions

$$\begin{aligned} e(\varphi,\sigma) &\equiv \frac{E}{awT} = \frac{|g(\varphi,\sigma) - e^{-i\sigma\varphi}|}{\sigma\varphi}, \\ c(\varphi,\sigma) &\equiv \frac{C}{(awT)\cdot(wL)} = sN_{op}\frac{1}{\sigma\varphi^2}. \end{aligned} \tag{16}$$

Optimizing the performance of a given scheme (i.e. for given values of s, N_{op}) for a given problem amounts to requiring that the computational cost be minimum for a given error level; this can be done by specifying a target level for the relative error, say ϵ, which implies

$$e(\varphi,\sigma) = \frac{\epsilon}{awT} \equiv \tilde{\epsilon}, \tag{17}$$

and then minimizing the computational cost, i.e. finding the minimum value of the cost function $c \sim 1/(\sigma\varphi^2)$ compatible with the constraint (17), as well as with the stability limitation $|g(\varphi,\sigma)| \leqslant 1\ \forall\varphi$; the latter constraint yields a limitation on the maximum value of the Courant number, $\sigma \leqslant \sigma_{max}$, which depends upon both the spatial and temporal discretizations.

The interpretation of the optimization problem is made particularly simple from inspection of the iso-lines of the normalized error and normalized cost functions in the φ, σ plane, as done in Fig. 1 for some representative spatial discretizations with three-stage, third-order Runge–Kutta time integration. For any specified value of $\tilde{\epsilon}$ one can in general find a pair of values $(\varphi^*(\tilde{\epsilon}), \sigma^*(\tilde{\epsilon}))$ that minimize $1/(\sigma\varphi^2)$, and which correspond

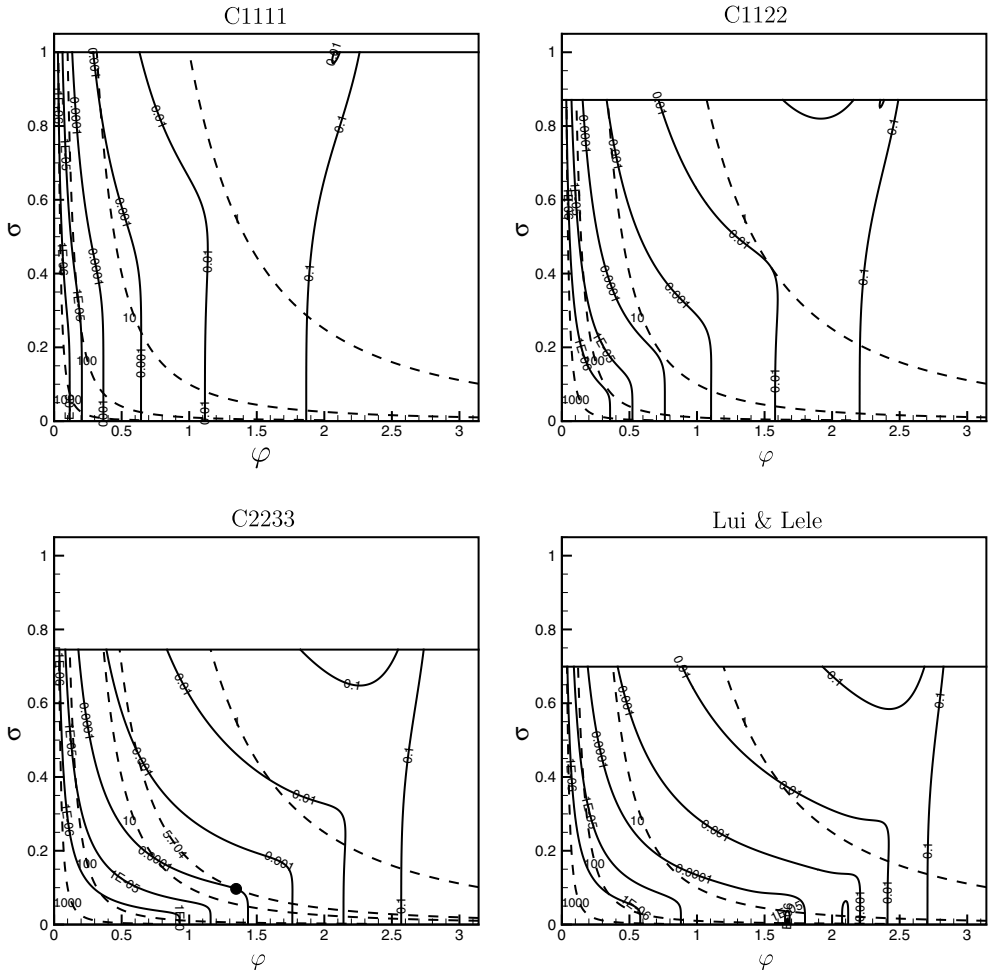

Fig. 1. Iso-contours of normalized 'local' error function $e(\varphi,\sigma)$ (solid lines) and normalized (one-dimensional) cost function $1/(\sigma\varphi^2)$ (dashed lines). RK3 time integration. The upper boundary corresponds to $\sigma = \sigma_{\max}$. The black dot indicates optimal working conditions for $\tilde{\epsilon} = 10^{-4}$.

to the tangency points of the two families of curves depicted in Fig. 1. The corresponding normalized (optimal) cost is given by

$$\tilde{c}(\tilde{\epsilon}) = c(\varphi^*(\tilde{\epsilon}), \sigma^*(\tilde{\epsilon})) = sN_{\mathrm{op}} \frac{1}{\sigma^* \varphi^{*2}}. \tag{18}$$

After having determined optimal values of φ^*, σ^*, one then obtains optimal values of the grid spacing and for the time step, which depend upon the target error level

$$h^*(\tilde{\epsilon}) = \varphi^*(\tilde{\epsilon})/w, \quad k^*(\tilde{\epsilon}) = \sigma^*(\tilde{\epsilon}) h^*(\tilde{\epsilon})/a. \tag{19}$$

For illustrative purposes, let us consider the C2233/RK3 scheme (for which $s = 3$, $N_{\mathrm{op}} = 17$), and assume as test problem the one-dimensional propagation of a sine wave with wavenumber $w = 10$ and wave speed $a = 1$ in a computational domain of extent $L = 2\pi$. If a maximum relative error $\epsilon = 10^{-2}$ on the computed solution is required at the time $T = 10$, to which corresponds a normalized error level $\tilde{\epsilon} = \epsilon/(awT) = 10^{-4}$, the cost minimization procedure would give (see Fig. 1, where the optimal point is reported as a black dot) $\varphi^* = 1.347$, $\sigma^* = 0.0967$; the associated 'optimal' normalized cost (as from Eq. (18)) is $\tilde{c} = 290.7$. The optimal values for the grid spacing and for the time step, as computed from Eq. (19) are $h^* = 0.1347$ (and the corresponding number of grid cells would be $L/h^* \approx 47$), and $k^* = 0.0130$.

2.4. Optimal performance for multi-scale problems

When dealing with nonlinear propagation problems and/or with broadband signals, the primary effect is to have a whole range of spatial scales (wavenumbers), say $0 \leqslant w \leqslant \overline{w}$, and propagation velocities, say $0 \leqslant a \leqslant \overline{a}$. In this case the formula for the relative error, being $n = (\bar{a}\bar{w}T)/(\bar{\sigma}\bar{\varphi})$, becomes

$$E = (\bar{a}\bar{w}T) \cdot \frac{|g(\varphi,\sigma) - \mathrm{e}^{-\mathrm{i}\sigma\varphi}|}{\bar{\sigma}\bar{\varphi}}, \tag{20}$$

while the cost function becomes

$$C \sim (\bar{a}\bar{w}T) \cdot (\bar{w}L) \cdot \bar{c}(\bar{\varphi},\bar{\sigma}), \tag{21}$$

with

$$\bar{c}(\bar{\varphi},\bar{\sigma}) = sN_{\mathrm{op}} \frac{1}{\bar{\sigma}\bar{\varphi}^2}. \tag{22}$$

The accuracy requirement that we enforce in this case dictates that the relative error be less than a given threshold for all possible values of φ, σ, i.e.

$$E \leqslant \epsilon, \quad \forall(\varphi,\sigma) \in [0,\bar{\varphi}] \times [0,\bar{\sigma}], \tag{23}$$

where $\bar{\varphi} = \bar{w}h$ and $\bar{\sigma} = \bar{a}k/h$, which implies

$$\begin{aligned} \bar{e}(\bar{\varphi},\bar{\sigma}) &\equiv \frac{1}{\bar{a}\bar{w}T} \cdot \max_{(\varphi,\sigma)\in[0,\bar{\varphi}]\times[0,\bar{\sigma}]} E \\ &= \frac{1}{\bar{\sigma}\bar{\varphi}} \cdot \max_{(\varphi,\sigma)\in[0,\bar{\varphi}]\times[0,\bar{\sigma}]} |g(\varphi,\sigma) - \mathrm{e}^{-\mathrm{i}\sigma\varphi}| \leqslant \frac{\epsilon}{\bar{a}\bar{w}T} \equiv \tilde{\epsilon}. \end{aligned} \tag{24}$$

The only change from the single-scale case is the replacement of the normalized error function e in Eq. (17) with $\bar{e}$, as defined in Eq. (24). The iso-contour lines of $\bar{e}(\bar{\varphi},\bar{\sigma})$ are reported in Fig. 2 together with the iso-cost lines; such 'global' normalized error differs from the 'local' one (compare with Fig. 1) only near points of local extrema of $e(\varphi,\sigma)$. The interpretation goes along the same lines as for the single-scale case: for each value of $\tilde{\epsilon}$ there is a couple of values $(\bar{\varphi}^*(\tilde{\epsilon}), \bar{\sigma}^*(\tilde{\epsilon}))$ that minimize the cost. The corresponding normalized (optimal) cost is

$$\tilde{c}(\tilde{\epsilon}) = \bar{c}(\bar{\varphi}^*(\tilde{\epsilon}), \bar{\sigma}^*(\tilde{\epsilon})) = sN_{\mathrm{op}} \frac{1}{\bar{\sigma}^*\bar{\varphi}^{*2}}. \tag{25}$$

We point out that the accuracy requirement (23) implicitly attributes the same importance to all the flow scales; in some situations, however, such as for numerical simulation of turbulent flows, one may wish to accurately compute the energy containing scales, and perhaps relax the accuracy requirement for the smaller ones. This might be accounted for by introducing an appropriate weighing function in wavenumber space in the definition of the error; we leave it for future work.

It is important to stress that the problem of optimal performance of a given scheme can be equivalently cast in terms of achieving minimal error for given computational cost; is that case one would specify an affordable level of computational cost, and try to determine the lowest compatible error. Of course, the resulting error–cost relationship would be exactly the same as the one expressed in Eq. (25), and the optimal reduced wavenumber and Courant number would be determined as a function of cost, being $\tilde{\epsilon} = \tilde{\epsilon}(\tilde{c})$. The interpretation of the optimization problem in terms of cost is particularly important for multi-scale problems, since the actual error incurred in numerical simulations depends upon the energy content of the solution in wavenumber space, and therefore one may expect that the error map in the (φ,σ) plane to depend upon the specific solution that one is computing. On the contrary, the normalized cost metric does not depend on the details of the solution, but rather is invariant in the (φ,σ) plane by virtue of its definition. We will go back to this point and provide illustrative examples when discussing the application of the present theory to problems of practical relevance in Section 6.

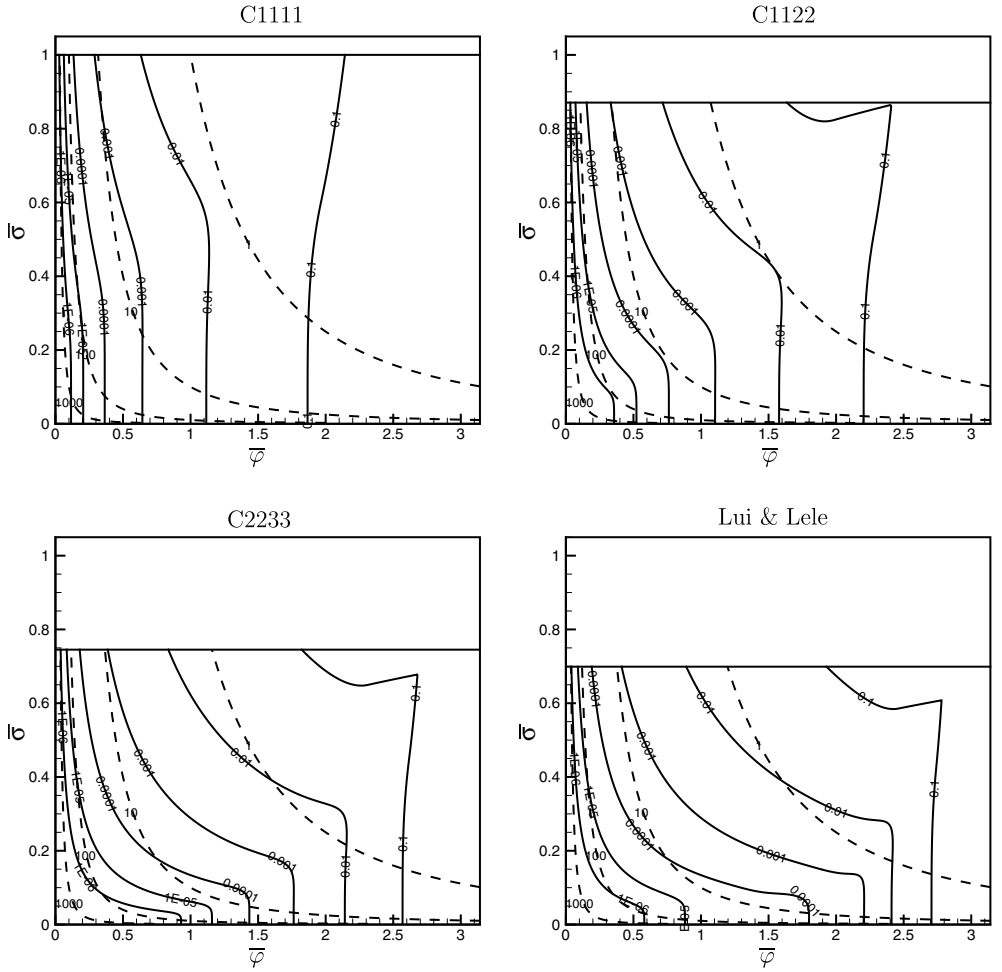

Fig. 2. Iso-contours of normalized 'global' error function $\bar{e}(\bar{\varphi},\bar{\sigma})$ (solid lines) and normalized (one-dimensional) cost function $1/(\bar{\sigma}\bar{\varphi}^2)$ (dashed lines). RK3 time integration. The upper boundary corresponds to $\bar{\sigma}=\sigma_{\max}$.

2.5. Multi-dimensional problems

The effect of the number of space dimensions can be partially accounted for in the analysis by assuming again the linear advection equation as working model, and consider monochromatic plane wave solutions. As shown in Ref. [8], although waves propagate non-isotropically on a finite mesh, the discrete propagation properties in directions not aligned with the grid lines only depend upon the 'one-dimensional' spectral properties of the scheme (i.e. its approximate dispersion relation), and the error is maximum for waves propagating along the coordinate directions [8,2]. We therefore assume: (i) uniform (and equal) grid spacing in the coordinate directions; and (ii) wave propagation along the grid lines. Under these assumptions, one can entirely borrow the one-dimensional analysis carried out in Section 2 but for the definition of the cost function, which must account for the fact that the total number of points is now V/h^{n_D}, where V is the volume of the computational domain, and n_D is the number of spatial dimensions, yielding

$$C \sim (\bar{a}\bar{w}T)\cdot(\bar{w}^{n_D}V)\cdot\bar{c}_{n_D}(\bar{\varphi},\bar{\sigma}), \tag{26}$$

where the normalized cost function is

$$\bar{c}_{n_D}(\bar{\varphi},\bar{\sigma}) = sN_{op}\frac{1}{\bar{\sigma}\bar{\varphi}^{n_D+1}}, \tag{27}$$

in the place of Eqs. (21) and (22).

3. Efficiency comparison

In order to compare the performance of different schemes it is sufficient to analyze the (normalized) error vs cost relation, accounting for the operation count estimate reported in Ref. [2]. The results of the analysis are shown in Fig. 3 for various spatial discretizations coupled with three-stage, third-order Runge–Kutta time integration (RK3); the figure reveals some interesting features, some of which were already reported in

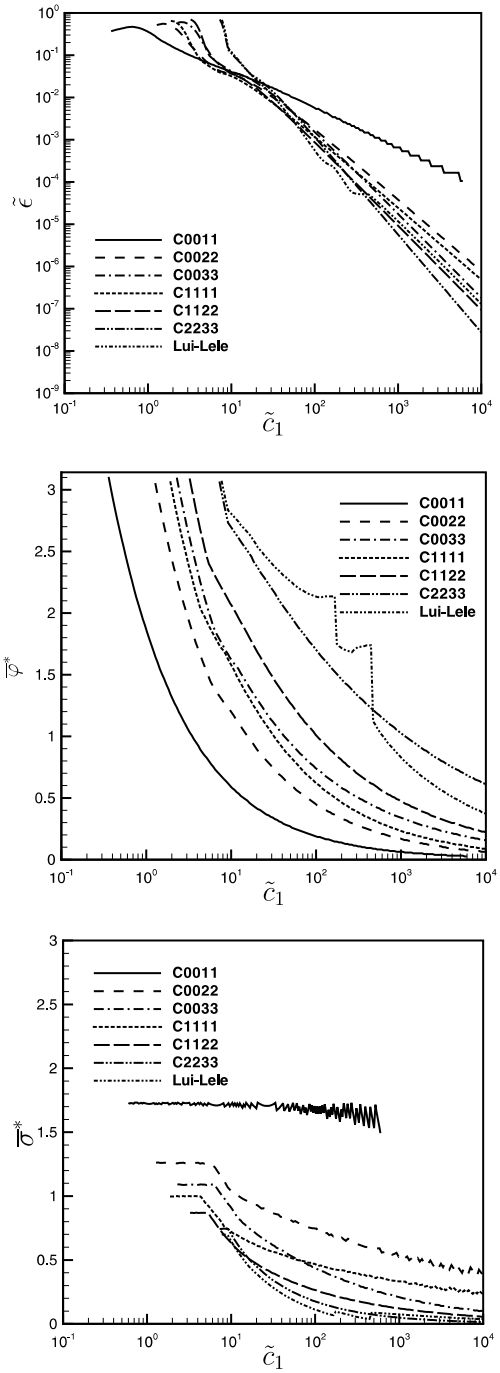

Fig. 3. 'Optimal' error, reduced wavenumber and Courant number as a function of cost for various spatial discretizations coupled with RK3 time integration in one space dimension.

Ref. [2]. In f rve that for normalized err mance; howe ccuracy is required, high-or the pentadia cheme of Lui and Lele offe tenth-order, ntadiagonal scheme (C2233) What is perh ing to see is that, while for coa mance is ach nt numbers close to the stabili sought for, c nce is achieved for small Coura vation may p idance for CFD and CAA pract grounds, by e conveniently close to the one d

We point in Fig. 3 we only report the efficie equally well mpact) upwind schemes, which ma shock-captur see, e.g. Ref. [10]); the main resul schemes are at centered schemes having the same for CAA ap also Refs. [2,3]).

3.1. Effect of tion

In order t the effect of the time integration scheme, error map an ency analysis for the same spatial discretizat

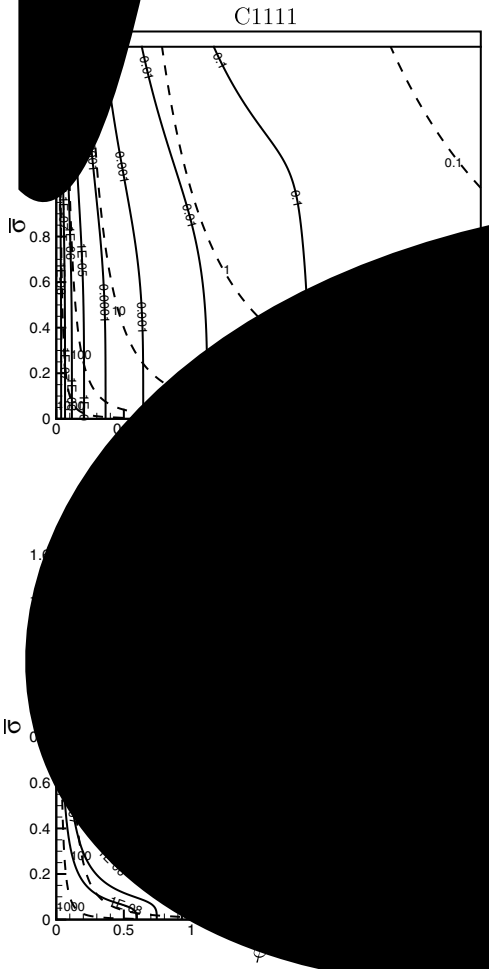

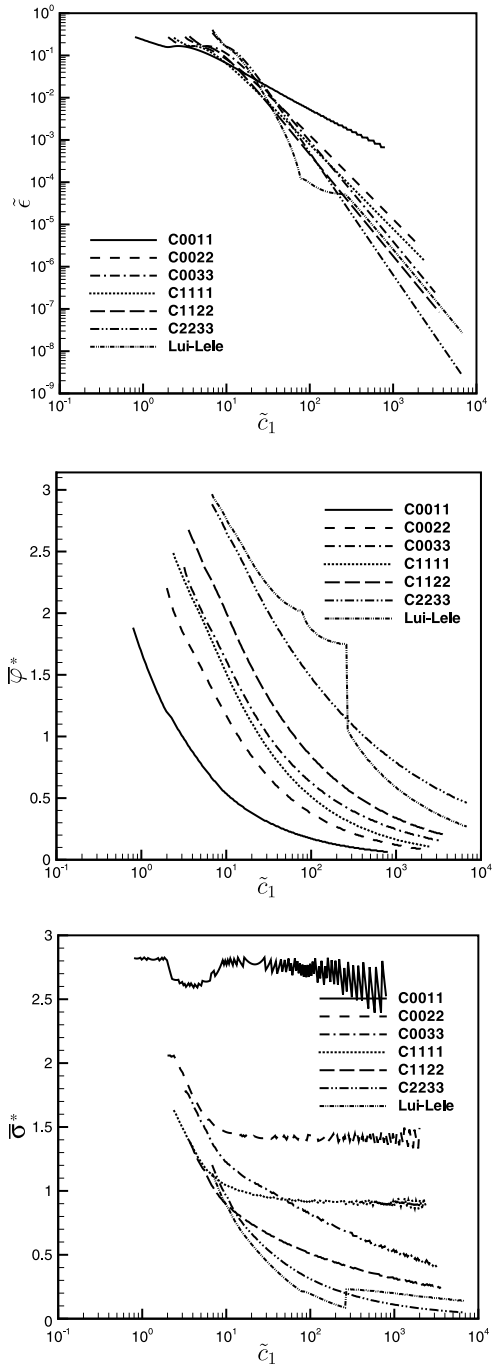

Fig. 5. 'Optimal' error, reduced wavenumber and Courant number as a function of cost for various spatial discretizations coupled with RK4 time integration in one space dimension.

Runge–Kutta (RK4) time integration. As expected [7], increased accuracy more than outweights increased computational cost, and indeed all schemes are found to perform more efficiently with RK4 time integration. It is also interesting to observe an increased effect of spatial discretization optimization, which promises up to 50% CPU time saving in this case (in a narrow range of error levels).

3.2. Multi-dimensional problems

With regard to the issue of optimal performance for multi-dimensional problems, recalling the discussion related to Fig. 1, and noticing that the only difference of the 'multi-dimensional' cost function from the 'one-dimensional' one is the change in the slope of the iso-cost hyperbolas (see Eq. (27)), one may expect that the optimal values of $\bar{\varphi}$ and $\bar{\sigma}$ for a given error level do not significantly differ from those found in the one-dimensional analysis. The data reported in Fig. 6 show that this is indeed the case: the conclusion is that schemes capable to operate at higher values of the reduced wavenumber are favoured even more for multi-dimensional simulations, because of the increased importance of $\bar{\varphi}$ in the cost metric (Eq. (27)). Accordingly, high-order and optimized schemes are expected to yield greater advantage over low-order ones for a given error level. The validity of these arguments will be further discussed in Section 6, where sample results of multi-dimensional calculations are presented.

4. Error analysis

The 'local' normalized error function $e(\varphi, \sigma)$ defined in Eq. (17) can be readily related to the error definitions used in previous studies. Indeed, for $\sigma \to 0$, since $g(\varphi, \sigma) = 1 - \mathrm{i}\sigma\Phi(\varphi) + \mathrm{O}(\sigma^2)$, and $\mathrm{e}^{-\mathrm{i}\sigma\varphi} = 1 - \mathrm{i}\sigma\varphi + \mathrm{O}(\sigma^2)$, we have

$$e(\varphi, \sigma) \overset{\sigma\to 0}{\to} |\Phi(\varphi) - \varphi|/\varphi \equiv e_0(\varphi), \tag{28}$$

which is the definition of the relative error in wavenumber space used by Lele [8] assuming zero time integration error. However, note that Lele only considered central schemes, for which $\Phi \in \mathbb{R}$, while the present definition equally well applies to upwind schemes, for which Φ has non-zero imaginary part. On the other hand, neglecting the spatial discretization error (i.e. setting $\Phi = \varphi$) one obtains the definition of time discretization error used by Hu et al. [7]

$$e_t(z) = \frac{1}{z}\left|\sum_{m=0}^{s} \gamma_m(-\mathrm{i}z)^m - \mathrm{e}^{-\mathrm{i}z}\right|, \tag{29}$$

where $z = \sigma\varphi$; however, note that Hu et al. consider only the numerator of Eq. (29) as a measure of the error. The geometry of the iso-error curves in Fig. 1 indeed indicates that for small Courant numbers the error is uniquely a function of the modified wavenumber, as given by Eq. (28), while at larger σ the curves bend becoming equilateral hyperbolas, i.e. the error becomes a function of z, as given by Eq. (29); with good one has

$$e(\varphi, \sigma) \approx \max(e_0(\varphi), e_t(\sigma\varphi)), \tag{30}$$

as shown in Fig. 7a.

With regard to the 'global' error, as defined in Eq. (24), the approximation (30) yields, after some algebra

$$\bar{e}(\bar{\varphi}, \bar{\sigma}) \approx \max(\bar{e}_0(\bar{\varphi}), \bar{e}_t(\bar{\sigma}\bar{\varphi})), \tag{31}$$

where the 'global' spatial error is given by

$$\bar{e}_0(\bar{\varphi}) = \frac{1}{\bar{\varphi}} \max_{0\leqslant\varphi\leqslant\bar{\varphi}} |\Phi(\varphi) - \varphi|, \tag{32}$$

and the 'global' temporal error is

$$\bar{e}_t(\bar{z}) = \frac{1}{\bar{z}} \max_{0\leqslant z\leqslant\bar{z}} \left|\sum_{m=0}^{s} \gamma_m(-\mathrm{i}z)^m - \mathrm{e}^{-\mathrm{i}z}\right|, \tag{33}$$

with $\bar{z} = \bar{\sigma}\bar{\varphi}$. Fig. 7b shows that Eq. (31) is a good approximation of the 'true' global error.

The condition of optimal performance for a given error level (say $\tilde{\epsilon}$) implies tangency of the associated iso-error curve with the normalized iso-cost curves $\bar{c}_{n_\mathrm{D}} \sim 1/(\bar{\sigma}\bar{\varphi}^{n_\mathrm{D}+1})$; this occurs near the bend of the $\bar{e}(\bar{\varphi}, \bar{\sigma}) = \tilde{\epsilon}$ graph, and, according to the approximation (30), at the point where $\bar{e}_0(\bar{\varphi}) = \bar{e}_t(\bar{z}) = \tilde{\epsilon}$. The problem of deter-

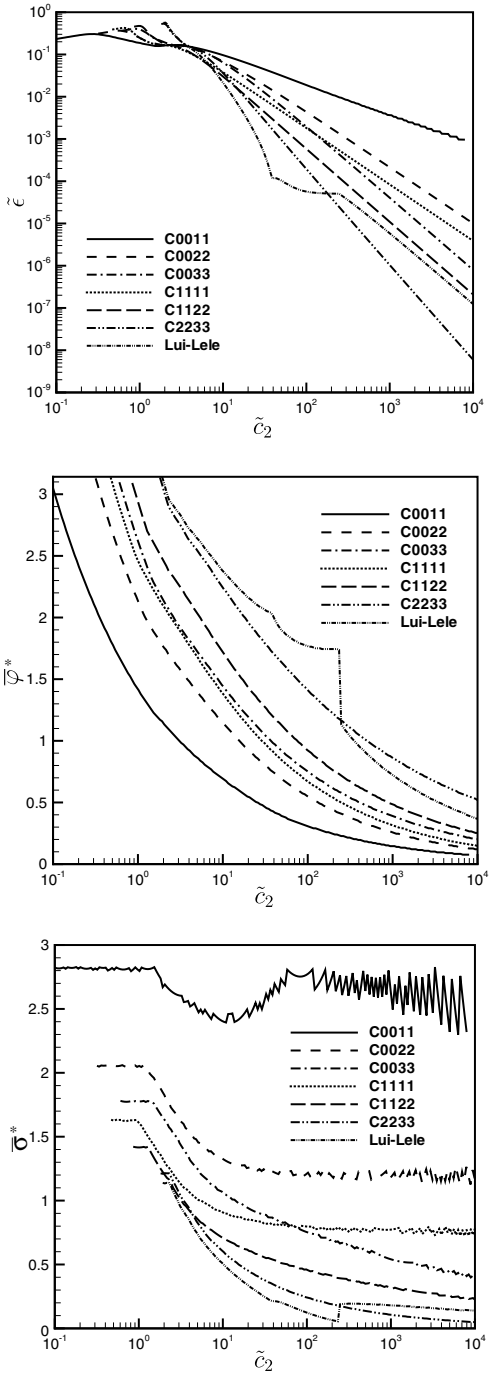

Fig. 6. 'Optimal' error, reduced wavenumber and Courant number as a function of cost for various spatial discretizations coupled with RK4 time integration in two space dimensions.

mining the optimal performance of a given scheme can therefore be approximately decoupled into two sub-problems, whereby the influence of space- and time-discretizations are considered separately, by: (i) computing the optimal reduced wavenumber according to

$$\bar{\varphi}^*(\tilde{\epsilon}) = \bar{e}_0^{-1}(\tilde{\epsilon}); \tag{34}$$

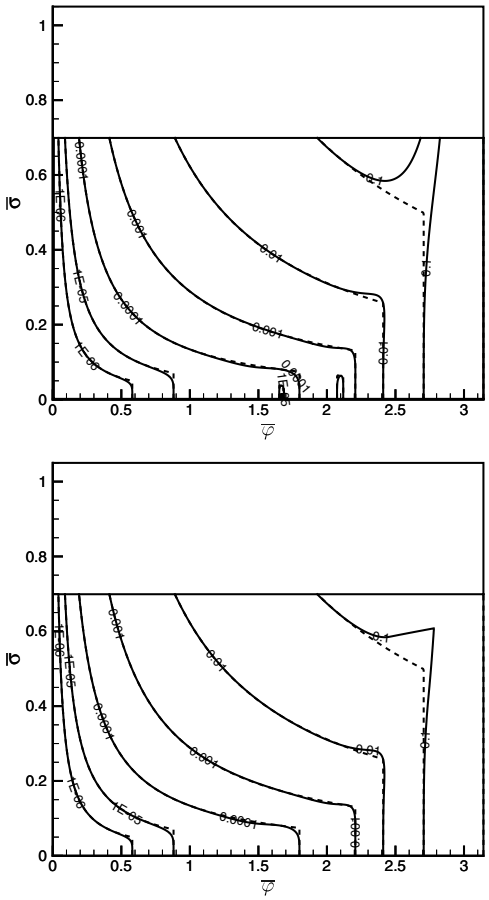

Fig. 7. Iso-contours of normalized 'local' error function $e(\varphi, \sigma)$ (a) and 'global' error function $\bar{e}(\bar{\varphi}, \bar{\sigma})$ (b) for Lui and Lele scheme with RK3 time integration. Dashed lines represent the corresponding approximations, as from Eqs. (30) and (31).

and (ii) computing the optimal Courant number from

$$\bar{\sigma}^*(\tilde{\epsilon}) = \bar{z}^*(\tilde{\epsilon})/\bar{\varphi}^*(\tilde{\epsilon}), \quad \bar{z}^*(\tilde{\epsilon}) \equiv \bar{e}_t^{-1}(\tilde{\epsilon}); \tag{35}$$

the associated normalized cost is

$$\tilde{c}(\tilde{\epsilon}) = \bar{c}_{n_D}(\bar{\varphi}^*(\tilde{\epsilon}),\ \bar{\sigma}^*(\tilde{\epsilon})) = sN_{\mathrm{op}} \frac{1}{\bar{\sigma}^* \bar{\varphi}^{*n_D+1}}. \tag{36}$$

For this reason spatial and temporal discretizations can (only approximately) be considered separately in the error analysis.

It is interesting to observe that the analysis carried out for spatial discretizations by Lele [8] can be recast in terms of the present formalism by defining the global spatial error as

$$\bar{e}_0^L(\bar{\varphi}) = \max_{0 \leqslant \varphi \leqslant \bar{\varphi}} \left(\frac{|\Phi(\varphi) - \varphi|}{\varphi} \right); \tag{37}$$

the optimal value of the reduced wavenumber computed according to Eq. (34) then represents the first value of $\bar{\varphi}$ for which $\bar{e}_0^L = \tilde{\epsilon}$, and in Lele's terminology it is labeled 'resolving efficiency' of the scheme, i.e. the range of well-resolved wavenumbers (to be more precise, Lele defines the resolving efficiency as $e_1(\tilde{\epsilon}) = \bar{\varphi}^*(\tilde{\epsilon})/\pi$). Note that in principle Eq. (37) differs from the present definition of the spatial error function, as given in Eq. (32), which, as we have shown, consistently derives from a sound definition of the overall error; in practice, however, the difference between the two definitions is limited to those intervals of the φ axis where $|\Phi(\varphi) - \varphi|$ is decreasing, and it does not affect the evaluation of the optimal reduced wavenumber.

5. Optimization criteria

On the basis of the discussion reported in the previous section, optimized finite-difference schemes can in principle be tailored for a specified target error level trying to maximize (see Eq. (36)) $\bar{\varphi}^*(\tilde{\epsilon})$ and $\bar{z}^*(\tilde{\epsilon})$, which amounts to separately optimize (for the same error level $\tilde{\epsilon}$) the space and time-discretization schemes.

5.1. Optimized space discretizations

The optimization of a scheme for spatial discretization is achieved by maximizing its 'spatial resolving efficiency' $\bar{\varphi}^*$ for a given value of the normalized error. For the sake of the analysis, let us consider a family of sixth-order compact difference approximations that satisfy Eq. (7), with $Q = R = 2$, $q = r = 3$, and

$$\begin{cases} a_3 = -a_{-3} = \frac{1}{60} + \frac{1}{5}\alpha_2 - \frac{1}{20}\alpha_1, \\ a_2 = -a_{-2} = -\frac{3}{20} + \frac{31}{30}\alpha_2 + \frac{8}{15}\alpha_1, \\ a_1 = -a_{-1} = \frac{3}{4} - \frac{5}{3}\alpha_2 + \frac{1}{12}\alpha_1, \end{cases} \tag{38}$$

where $\alpha_1 = \alpha_{-1}$ and $\alpha_2 = \alpha_{-2}$ are two free parameters. The specific choice $\alpha_1 = 1/2$, $\alpha_2 = 1/20$ yields the only tenth-order scheme in the family (C2233). We have attempted to find members of this family of schemes that maximize the resolving efficiency as a function of the normalized error level $\tilde{\epsilon}$. The optimal values of the coefficients α_1 and α_2 thus obtained are plotted in Fig. 8, and reported in tabular form for representative values of $\tilde{\epsilon}$ in Table 1; in the table we also report data on the resolving efficiency of the (non-optimized) C2233 scheme. It is evident that optimized spatial discretizations tailored for a specific error level in principle outperform C2233, yielding 40–50% increase in the spatial resolving efficiency. Fig. 8 also indicates that the optimal coefficients vary significantly with the error level, and that the optimal resolving efficiency may approach π (i.e. waves can be resolved with almost two points-per-wavelength) at large levels of the error. It is interesting to observe that the Lui and Lele scheme (which has $\alpha_1 = 0.5381301488732363$, $\alpha_2 = 0.066633190123881123$) very nearly belongs to this class of optimal schemes, and attains optimal performance for an error level $\tilde{\epsilon} \approx 7 \times 10^{-5}$.

5.2. Optimized time discretizations

The optimization of schemes for time integration is achieved by maximizing $\bar{z}^*$, which can be interpreted as a 'temporal resolving efficiency', for a given value of the normalized error, under the stability constraint

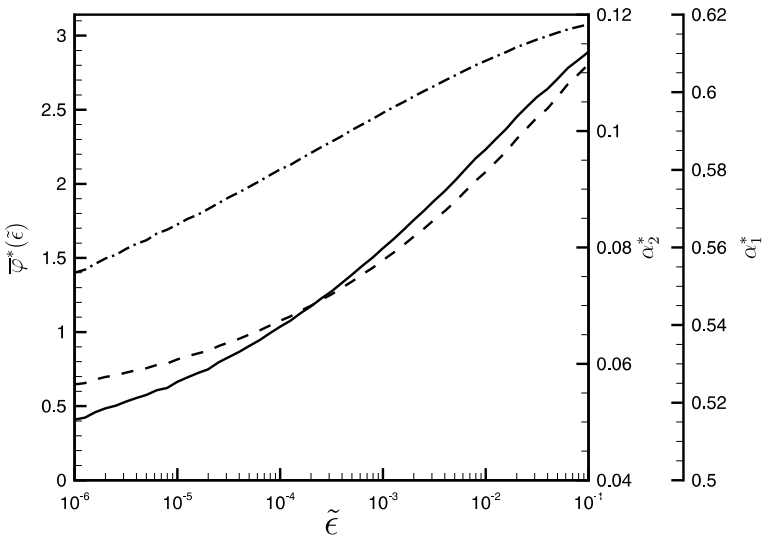

Fig. 8. Optimal values of coefficients α_1 (solid line), α_2 (dashed line), and 'spatial resolving efficiency' $\bar{\varphi}^*$ (dash-dotted line) for sixth-order, pentadiagonal optimized compact scheme.

Table 1
Coefficients and performance of space-optimized schemes for various target errors

$\tilde{\epsilon}$	α_1	α_2	$\bar{\varphi}^*$	$\bar{\varphi}^*$ (C2233)
10^{-5}	0.5253882280	0.06077763382	1.726	1.160
10^{-4}	0.5396065722	0.06742221409	2.098	1.436
10^{-3}	0.5598183379	0.07781267648	2.478	1.764

$$\left|\sum_{m=0}^{s}\gamma_m(-\mathrm{i}z)^m\right| \leqslant 1. \tag{39}$$

We have considered as representative example a four-stage, second-order Runge–Kutta scheme, i.e. set $\gamma_1 = 1$, $\gamma_2 = 1/2$, and left two free parameters γ_3, γ_4. The results of the analysis are plotted in Fig. 9 and reported in tabular form in Table 2; in the table we also report data on the resolving efficiency of the non-optimized RK4 scheme. Optimal time integration schemes have smaller values of γ_3, γ_4 than the non-optimized Runge–Kutta scheme, which has $\gamma_3 = 1/6$, $\gamma_4 = 1/24$, and outperform RK4 yielding 20–40% increase in the temporal resolving efficiency. We point out that the four-stage Runge–Kutta scheme proposed by Hu et al. [7], which has $\gamma_3 = 0.162997$, $\gamma_4 = 0.0407574$, does not belong to this class of optimized time integration schemes, and has not been considered for comparison here since it does not satisfy the constraint (39), which makes it unsuitable for long time integrations.

5.3. Performance of optimized schemes

In order to demonstrate the potential effect of the proposed optimization strategy we have considered a series of target error levels $\tilde{\epsilon} = 10^{-3}, 10^{-4}, 10^{-5}$, and constructed finite-difference schemes combining space- and time-optimized schemes tailored for the same error level; in our notation `epsm`*n*`-opt` denotes optimized

Table 2
Coefficients and performance of time-optimized schemes for various target errors

$\tilde{\epsilon}$	γ_3	γ_4	$\bar{z}^*$	$\bar{z}^*$ (RK4)
10^{-5}	0.1661162857	0.04107313943	0.268	0.187
10^{-4}	0.1653056266	0.04030427254	0.437	0.332
10^{-3}	0.1636462002	0.03863560284	0.709	0.590

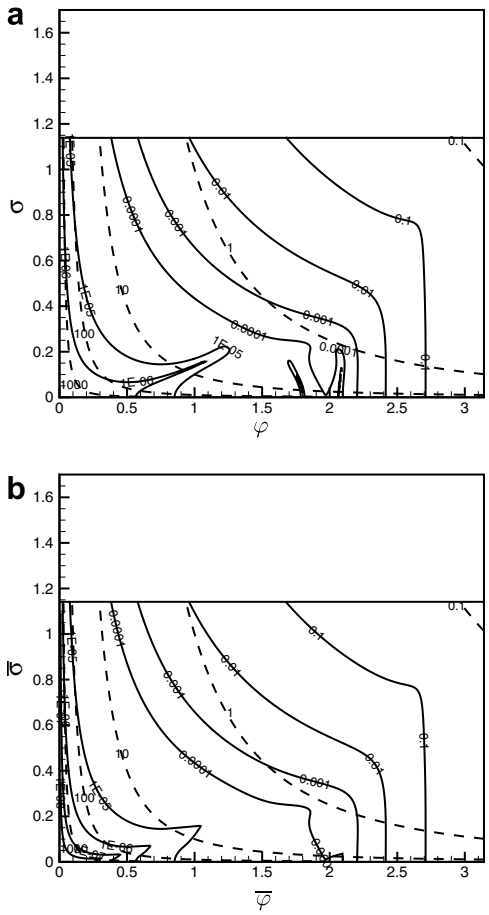

Fig. 10. Iso-contours of normalized 'local' (a) and 'global' (b) error function $\bar{e}(\bar{\varphi},\bar{\sigma})$ (solid lines) and normalized (one-dimensional) cost function $1/(\bar{\sigma}\bar{\varphi}^2)$ (dashed lines) for `epsm4-opt` optimized scheme. The upper boundary corresponds to $\bar{\sigma}=\sigma_{\max}$.

schemes tailored for a normalized error level $\tilde{\epsilon}=10^{-n}$. The error map obtained with the `epsm4-opt` scheme is depicted in Fig. 10, which confirms the occurrence of an extended range of well-resolved wavenumbers in coincidence of its design error level $\tilde{\epsilon}=10^{-4}$, over its non-optimized counterpart (C2233/RK4, see Fig. 4). The nominal performance of optimized schemes (in two space dimensions) is illustrated in Fig. 11 and Table 3; the values of optimal cost, reduced wavenumber and Courant number deduced from Tables 1 and 2 fairly agree with the ones obtained from the exact cost minimization procedure. The most evident result is that space- and time-optimized schemes can yield substantial savings, of the order of 60–70% in a decade around their design error level, compared to the corresponding non-optimized scheme (C2233/RK4). The main effect of optimization is to increase the range of well-resolved wavenumbers (i.e. $\bar{\varphi}^*(\tilde{\epsilon})$), while the optimal Courant number does not vary significantly compared to the non-optimized scheme.

6. Applications

In order to demonstrate the practical usefulness of the concept of optimal performance of finite-difference schemes, and to illustrate the actual advantages provided by optimized schemes, in the present section we have carried out numerical simulations of the two-dimensional acoustics equations, which can be written in conservation form as follows:

$$\frac{\partial \mathbf{q}}{\partial t}+\frac{\partial \mathbf{f}}{\partial x}+\frac{\partial \mathbf{g}}{\partial y}=0, \tag{40}$$

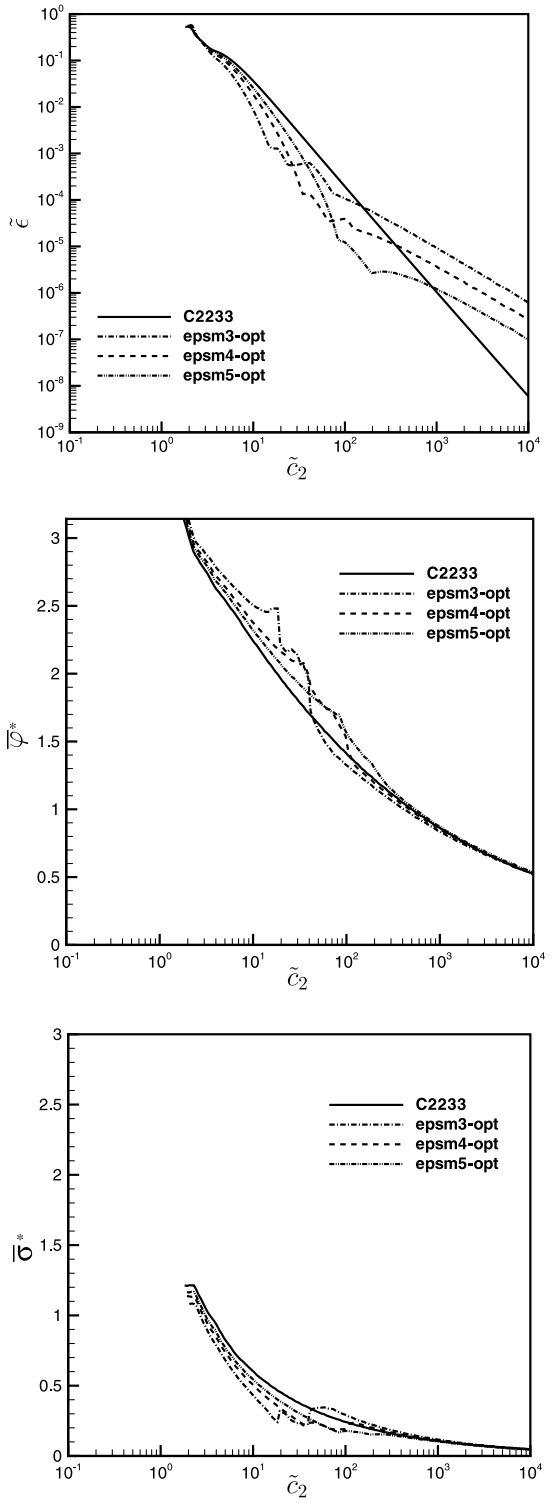

Fig. 11. 'Optimal' error, reduced wavenumber and Courant number as a function of cost for space- and time-optimized schemes in two space dimensions.

where $\mathbf{q} = [u, v, p]^{\mathrm{T}}$, $\mathbf{f} = [p, 0, u]^{\mathrm{T}}$, $\mathbf{g} = [0, p, v]^{\mathrm{T}}$. Working in such linear environment yields the significant advantage of having a number of exact solutions to exploit for quantitative analysis. Preliminary simulations

Table 3
Performance of space- and time-optimized schemes for various target errors in two space dimensions

Scheme	$\sigma_{\max}$	$\tilde{\epsilon}$	$\bar{\varphi}^*$	$\bar{z}^*$	$\tilde{c}_2$	$\Delta\%$
`epsm5-opt`	1.1694	10^{-5}	1.512	0.266	111.87	69.55
`epsm4-opt`	1.1387	10^{-4}	1.841	0.429	46.784	65.00
`epsm3-opt`	1.0863	10^{-3}	2.209	0.693	20.108	59.03

$\Delta\%$ denotes percent cost reduction over non-optimized reference scheme (C2233/RK4).

have been performed on a computational domain $[-10; 10]\times[-10; 10]$ on a cartesian uniformly spaced grid with $h_x = h_y = h$, for sinusoidal monochromatic acoustic waves propagating in the positive-x direction, with initial conditions

$$p_0(x,y) = \sin(2\pi n x), \quad u_0(x,y) = 0, \quad v_0(x,y) = 0, \tag{41}$$

and periodic boundary conditions; the calculations have been time-advanced up to a time $T = 1$. The exact solution ($\tilde{\mathbf{q}}$) of the problem is

$$\begin{cases} \tilde{p}(x,y,T) = \cos(2\pi n T)\sin(2\pi n x), \\ \tilde{u}(x,y,T) = -\sin(2\pi n T)\cos(2\pi n x), \\ \tilde{v}(x,y,T) = 0. \end{cases} \tag{42}$$

Extensive simulations have been carried out varying both n (which controls the wavenumber of the disturbances) and h (the mesh spacing); let the relative error at time T be defined as

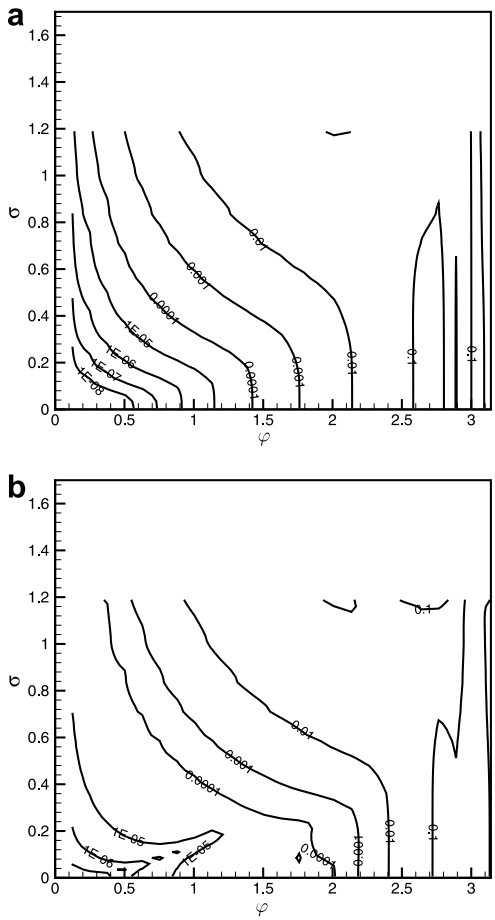

Fig. 12. Computed iso-contours of normalized error for 1D wave propagation test case: (a) C2233/RK4 and (b) `epsm4-opt`.

$$E = \left[\frac{\sum_{i,j} |\mathbf{q}_{i,j} - \tilde{\mathbf{q}}(x_i, y_j)|^2}{\sum_{i,j} |\mathbf{q}_0(x_i, y_j)|^2} \right]^{1/2}, \tag{43}$$

in accordance with (14), and noticing that for the present problem the relevant wavenumber is $w = 2\pi n$, and the propagation speed of disturbances is $a = 1$, we have plotted the computed normalized error, as defined in (17), as a function of $\varphi = wh$, $\sigma = ak/h$ in Fig. 12 for the C2233/RK4 and the optimized `epsm4-opt` schemes. The error maps thus obtained are almost identical to the theoretical ones, shown in Figs. 4 and 10, and clearly show that the results derived for the scalar, one-dimensional case, including optimal choice of mesh spacing and time step, automatically apply to the present, single-scale vector problem.

Going one step further, we have considered the propagation of monochromatic acoustic disturbances in the $\pm 45°$ directions, with initial conditions

$$p_0(x, y) = \sin(2\pi n x) \sin(2\pi n y), \quad u_0(x, y) = 0, \quad v_0(x, y) = 0, \tag{44}$$

with periodic boundary conditions and in the same computational box as the first test case. An exact solution for the problem at time $T(= 1)$ is given by [4]

$$\begin{cases} \tilde{p}(x, y, T) = \cos(2\sqrt{2}\pi n T) \sin(2\pi n x) \sin(2\pi n y), \\ \tilde{u}(x, y, T) = -\sin(2\sqrt{2}\pi n T) \cos(2\pi n x) \sin(2\pi n y)/\sqrt{2}, \\ \tilde{v}(x, y, T) = -\sin(2\sqrt{2}\pi n T) \sin(2\pi n x) \cos(2\pi n y)/\sqrt{2}. \end{cases} \tag{45}$$

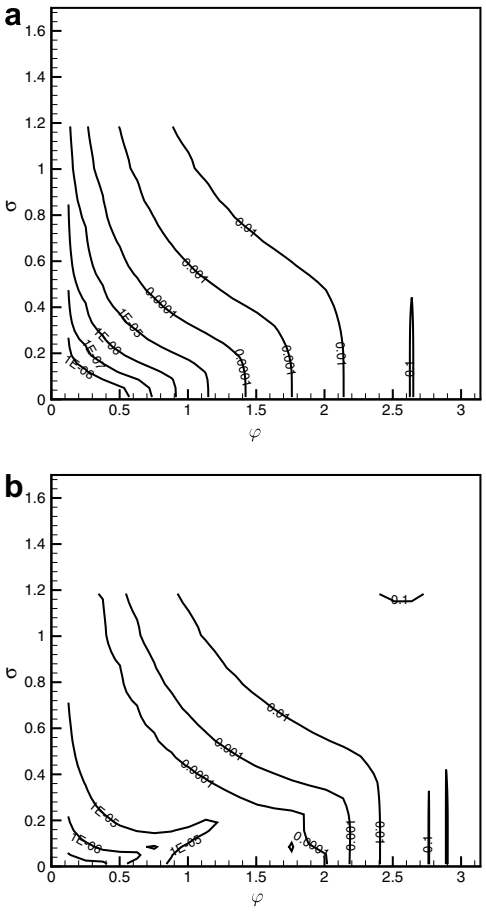

Fig. 13. Computed iso-contours of normalized error for 2D wave propagation test case: (a) C2233/RK4 and (b) `epsm4-opt`.

For this test case the relevant wavenumber is $w = 2\pi n\sqrt{2}$, and the relevant grid spacing (in the direction normal to the wave front) is $h/\sqrt{2}$. The results of computations performed at various n and h are reported in terms of distributions of the normalized L_2 error in Fig. 13. Once again, the maps very closely replicate the results obtained from the analysis of the scalar, one-dimensional advection equation, and the theoretical results entirely apply.

In practical problems one seldom has to deal with waves traveling only in one direction, nor has monochromatic waves. Therefore, the next level of complexity that we have considered is the isotropic propagation of a pressure pulse in an unbounded domain, with initial conditions

$$p_0(x,y) = \exp(-\alpha r^2), \quad u_0(x,y) = 0, \quad v_0(x,y) = 0, \tag{46}$$

where $r = (x^2 + y^2)^{1/2}$, $\alpha = \log 2/r_0^2$, and which has the following exact solution at time T [5]

$$\begin{cases} \tilde{p}(x,y,T) = \frac{1}{2\alpha}\int_0^\infty \exp\left(-\frac{\xi^2}{4\alpha}\right)\cos(\xi T)J_0(\xi r)\xi\,\mathrm{d}\xi, \\ \tilde{u}(x,y,T) = \frac{x}{2\alpha r}\int_0^\infty \exp\left(-\frac{\xi^2}{4\alpha}\right)\sin(\xi T)J_1(\xi r)\xi\,\mathrm{d}\xi, \\ \tilde{v}(x,y,T) = \frac{y}{2\alpha r}\int_0^\infty \exp\left(-\frac{\xi^2}{4\alpha}\right)\sin(\xi T)J_1(\xi r)\xi\,\mathrm{d}\xi, \end{cases} \tag{47}$$

where J_0 and J_1 are, respectively, the zeroth- and first-order Bessel functions of the first kind. Approximate solutions for this test case have been computed for $r_0 = 1$ on the domain $[-10;\ 10]\times[-10;\ 10]$ at a time

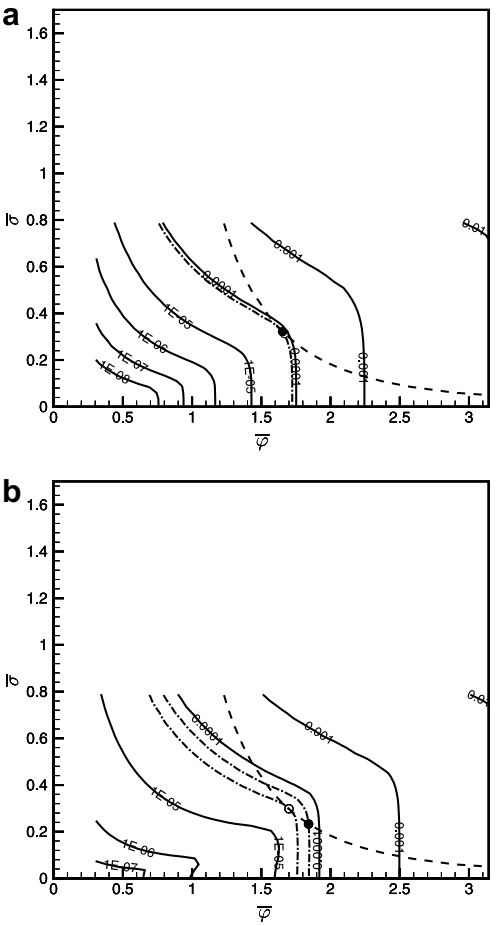

Fig. 14. Computed iso-contours of normalized error for 2D acoustic pulse propagation test case: (a) C2233/RK4 and (b) `epsm4-opt`. The dashed line corresponds to the iso-cost contour $\tilde{c}_2 = 46.784$. •, theoretical point of optimal performance; ∘, actual point of optimal performance.

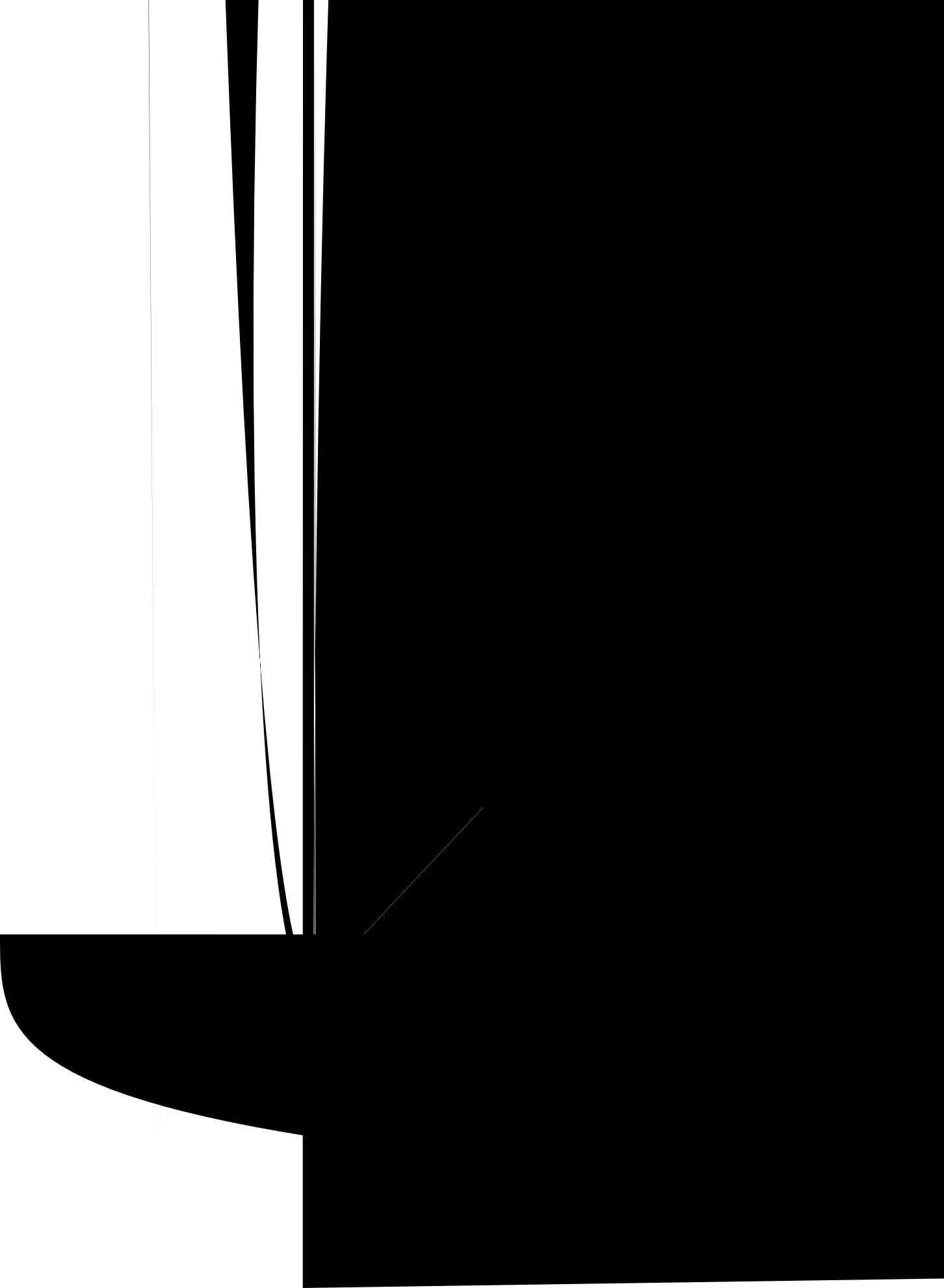

For the present test case a relevant wavelength for the pulse is $\lambda \approx 2r_0$, and accordingly we have set $\bar{w} = \pi$. The distributions of the normalized errors in the (φ, σ) plane for this test case are shown in Fig. 14; we observe that, although the shape of the iso-error curves again resembles Figs. 4 and 10b, the actual error, which is related to the occurrence of a whole spectrum of wavelengths in the solution and is made up of a weighted superposition of the errors associated to each harmonic, is clearly different from the theoretical one.

In order to show that some conclusions of the theoretical analysis still hold in the present case, in Fig. 15 we have reported the 'optimal' normalized error, reduced wavenumber and Courant number as a function of cost, as found from numerical simulations (i.e. as retrieved from the data reported in Fig. 14) for the C2233/RK4 and `epsm4-opt` schemes, and compared them with the corresponding theoretical predictions (already reported in Fig. 11). The figure confirms a lack of correspondence of the theoretical 'optimal' error-cost maps (lines) with the computed ones (lines + symbols); however, the qualitative behavior is the same, and in particular the optimized scheme is confirmed to be more efficient than its non-optimized counterpart in a certain range of cost (error) levels, even though the improvement is not as significant as expected. Although, as pointed out, the actual error levels do not correspond to the nominal ones, the optimal values of the reduced wavenumber and Courant number seem to obey (approximately) the same relationship upon the normalized cost $(\tilde{c}_2)$ as found from the theoretical analysis, as Fig. 15b–c clearly shows. In particular, the optimal working points for the C2233/RK4 scheme fall very close to the theoretical ones, while larger discrepancies are found for the `epsm4-opt` scheme. This observation confirms that the theory here developed can be used to infer the optimal operating conditions of a numerical scheme even for practical applications.

The procedure to determine the optimal computational settings in this case involves reasoning in terms of computational cost; let us consider, for example, a cost level $\tilde{c}_2 = 46.784$, which corresponds to the design cost for the `epsm4-opt` scheme (see Table 3) for a (nominal) normalized error level $\tilde{\epsilon} = 10^{-4}$; the associated optimal values of reduced wavenumber and Courant number for the `epsm4-opt` scheme are $\bar{\varphi}^* = 1.841$ and $\bar{\sigma}^* = 0.233$ (reported as a filled circle in Fig. 14b), which give an optimal grid spacing $h_x = h_y = h = \bar{\varphi}^*/\bar{w} = 0.586$ (that is approximately obtained with $N_x = N_y = 34$ cells), and an optimal time step $k = \bar{\sigma}^* h/a = 0.137$. Using such computational settings the `epsm4-opt` scheme yields a normalized error $\tilde{\epsilon} = 5.775 \times 10^{-5}$. We point out that the 'theoretical' optimal conditions are somewhat different from the 'true' optimal ones, as determined from the numerical simulations (reported as a hollow circle in Fig. 14b), which would give instead $\tilde{\epsilon} = 3.046 \times 10^{-5}$. For the same normalized cost level the C2233/RK4 scheme theoretically provides optimal performance at $\bar{\varphi}^* = 1.653$ and $\bar{\sigma}^* = 0.322$ (reported as a filled circle in Fig. 14a), that very closely correspond to the actual optimal values (hollow circle). The resulting values of the optimal grid spacing and time step are $h_x = h_y = h = 0.526$ (i.e. $N_x = N_y = 38$) and $k = 0.169$, for which the incurred error is $\tilde{\epsilon} = 8.439 \times 10^{-5}$. The improvement of the optimized scheme with respect to its non-optimized counterpart (in terms of error decrease for given cost) is ≈31.5%; for the same cost levels the theoretical error reduction would be ≈63.9%.

We may summarize the conclusions of the present analysis as follows: (i) the one-dimensional analysis carried out in the previous sections provides a useful guidance for determining the conditions for optimal performance (least cost) of a given scheme for a given cost level, even though some discrepancies are found with respect to the 'actual' optimal conditions for the optimized schemes; (ii) as expected, the actual error levels found in numerical simulations of multi-scale problems do depend upon the solution itself, and therefore cannot be accurately predicted from the outset; (iii) optimized schemes generally yield an improvement over non-optimized ones in terms of error decrease for given cost level (around their design value), however such decrease is heavily solution-dependent, and less than the theoretically predicted one.

7. Conclusions

In the present paper we have developed a rational procedure to gauge the performance of finite difference approximations for linear wave propagation problems, based on the analysis of the one-dimensional linear advection equation. After rigorously defining error and cost metrics, we have devised a roadmap to follow for optimal exploitation of computational resources: (i) for a given problem (characterized by a maximum expected wavenumber $\bar{w}$, maximum expected speed $\bar{a}$, and final time T), and for a given maximum error tolerance ϵ, the corresponding normalized error level is determined $\tilde{\epsilon} = \epsilon/(\bar{a}\bar{w}T)$; (ii) the most efficient space- and

time-discretization scheme for the specified error level is selected among existing ones or among the optimized ones proposed in Section 5 by analyzing the respective cost vs. error plots, as reported for example in Fig. 3a; (iii) for the selected scheme, optimal values of the reduced wavenumber ($\bar{\varphi}^*(\tilde{\epsilon})$) and of the Courant number ($\bar{\sigma}^*(\tilde{\epsilon})$) are obtained, for example from Fig. 3; (iv) optimal values for the grid spacing and the time step are obtained according to $h^*(\tilde{\epsilon}) = \bar{\varphi}^*(\tilde{\epsilon})/\bar{w}$, $k^*(\tilde{\epsilon}) = \bar{\sigma}^*(\tilde{\epsilon})h^*(\tilde{\epsilon})/\bar{a}$.

The theoretical analysis of the performance of various schemes has shown that high-order, and in particular optimized schemes, are in principle more efficient than low-order ones when high-fidelity solutions are sought for; this is even more so in several space dimensions. The analysis of the global error has shown that it is (approximately) made up of two terms, one associated with spatial discretization and one associated with time integration. This observation has led us to formulate general optimization criteria for the design of tailored space- and time-discretization schemes. An example carried out for a sixth-order pentadiagonal compact scheme with four-stage second-order Runge–Kutta time integration has shown that nominal reductions of the computational cost of the order of 60–70% are possible in a rather wide range of error levels. Numerical simulations of the two-dimensional acoustics equations have shown that the analysis directly applies single-scale multi-dimensional linear wave propagation problems.

Difficulties arise for the analysis in case of multi-dimensional systems of equations with various wave speeds and various angles; in such case the overall solution error is heavily dependent upon the solution itself, and (in a linear setting) it is a weighted average of the errors associated with each wavenumber and propagation angle; it is far from clear how the analysis, which only conveys information on a relevant lengthscale of the solution ($\bar{w}$), can help the selection of proper values of grid spacing and time step. Nevertheless, numerical simulations of an isotropic pressure pulse propagation in a two-dimensional environment have shown that the theory developed in the present paper still applies to some extent, provided the efficiency analysis is carried out in terms of obtaining the least error for given computational cost, the main reason being that the cost metric is not solution-dependent. For such test case optimized schemes are found to retain some advantage over non-optimized ones, even though the actual improvement may be far less than theoretical predictions.

We expect that the present analysis may also give some benefit for weakly nonlinear problems, because the leading order effects due variable wave speed and multiple flow scales are naturally accounted for; precise assessment of this statement is made difficult by the lack of exact solutions, and further efforts are required in this direction. We must also point out that the main focus of the paper was on the characterization of the propagation features of numerical schemes in an unbounded space, and the issue of boundary conditions has been left unaddressed. Proper enforcement of numerical boundary conditions is of utmost importance for the accuracy and stability of numerical algorithms, and future efforts will be concentrated on assessing the impact of boundary closures on the conclusions drawn in this study, and on designing suitable closures for optimized schemes.

References

[1] T. Colonius, Modeling artificial boundary conditions for compressible flow, Annu. Rev. Fluid Mech. 40 (2004) 315–345.
[2] T. Colonius, S.K. Lele, Computational aeroacoustics: progress on nonlinear problems of sound generation, Prog. Aerosp. Sci. 40 (2004) 345–416.
[3] J.A. Ekaterinaris, High-order accurate, low numerical diffusion methods for aerodynamics, Prog. Aero. Sci. 41 (2005) 192–300.
[4] R.W. Dyson, J.W. Goodrich, Automated approach to very high-order aeroacoustics computations, AIAA J. 39 (2001) 396–406.
[5] J.C. Hardin, J.R. Ristorcelli, C.K. Tam (Eds.), ICASE/LaRC Workshop on Benchmark Problems in Computational Aeroacoustics (CAA), NASA CP 3300, 1995 (unpublished).
[6] C. Hirsch, Numerical Computation of Internal and External Flows, Wiley, New York, 1988.
[7] F.Q. Hu, M.Y. Hussaini, J. Manthey, Low-dissipation and low-dispersion Runge–Kutta schemes for computational acoustics, J. Comput. Phys. 124 (1996) 177–191.
[8] S.K. Lele, Compact finite difference schemes with spectral-like resolution, J. Comput. Phys. 103 (1992) 16–42.
[9] C. Lui, S.K. Lele, Direct Numerical Simulation of Spatially Developing, Compressible, Turbulent Mixing Layers, AIAA Paper 2001-0291, 2001.
[10] S. Pirozzoli, Conservative hybrid compact-WENO schemes for shock–turbulence interaction, J. Comput. Phys. 178 (2002) 81–117.
[11] C.K.W. Tam, J.C. Webb, Dispersion–relation–preserving finite difference schemes for computational acoustics, J. Comput. Phys. 107 (1993) 262–281.
[12] R. Vichnevetsky, J.B. Bowles, Fourier Analysis of Numerical Approximations of Hyperbolic Equations, SIAM, Philadelphia, 1982.